ORIENTAL JOURNAL OF CHEMISTRY
An International Open Access, Peer Reviewed Research Journal
www.orientjchem.org
ISSN: 0970-020 X
CODEN: OJCHEG
2026, Vol. 42, No.(5):
Pg. 1996-2005

Valorization of Kaolin into a Zeolitic Eco-Adsorbent for the Removal of Bezaktiv Orange GO Dye

AFFOUÉ TINDO SYLVIE KONAN[1]*, N'GORAN SÉVÉRIN EROI[1], IGNACE CHRISTIAN M'BRA[1], ABOUBAKAR SIDDIK COULIBALY[1], KOFFI SIMÉON KOUADIO[1,2], SIRATA IBRAHIMA FRANCIS SORO[1], LYNDA EKOU[1] and TCHIRIOUA EKOU[1]

[1]Laboratoire de Thermodynamique et de Physico-Chimie du Milieu (LTPCM), Unité de Formation et de Recherche Sciences Fondamentales et Appliquées, Université Nangui ABROGOUA, 02 BP 801 Abidjan 02, Côte d'Ivoire
[2]Univ. Lille, CNRS, Centrale Lille, Univ. Artois, UMR 8181 - UCCS - Unité de Catalyse et Chimie du Solide, F-59000 Lille, France.
*Corresponding author E-mail: tindosylviekonan@yahoo.fr

http://dx.doi.org/10.13005/ojc/420519

(Received: July 17, 2026; Accepted: August 20, 2026)

ABSTRACT

This study focuses on the valorization of a kaolin-type clay for the hydrothermal synthesis of a zeolitic eco-adsorbent to remove Bezaktiv Orange GO from aqueous solution. X-ray diffraction (XRD) and Fourier-transform infrared spectroscopy (FTIR) analyses confirmed the formation of a hydrophilic porous structure typical of zeolites (P-type or sodalite) with a point of zero charge (pH_{PZC}) of 6.08. Adsorption experiments showed a maximum decolorization efficiency of 84.3% at pH = 2, driven by electrostatic interactions between the protonated surface and anionic dye molecules. Equilibrium was reached within 90 minutes. The kinetic study shows that the process follows the pseudo-second-order model (R_2 = 0.99), implying chemisorption, while the Freundlich isotherm indicates multilayer adsorption on a heterogeneous surface. Therefore, kaolin represents a low-cost, effective precursor for treating textile effluents.

Keywords: Clay, kaolin, zeolitic eco-adsorbent, adsorption, Bezaktiv Orange GO dye, textile effluents

INTRODUCTION

Industrial growth over recent decades has generated increasingly complex environmental problems, especially regarding water quality. Among the most concerning contaminants are synthetic dyes [1]. Used extensively in textiles, leather processing, cosmetics, food production, and pharmaceuticals, these compounds are engineered for high stability against light and chemical degradation. While this

This is an Open Access article licensed under a Creative Commons license: Attribution 4.0 International (CC- BY).
Published by Oriental Scientific Publishing Company © 2018

durability is desirable for industrial applications, it poses serious ecological risks. Their structural resistance and low biodegradability allow them to persist through conventional water treatment methods [2,3]. The release of colored wastewater into aquatic environments causes more than just visual pollution. By increasing water turbidity, these contaminants block sunlight penetration, thereby reducing the photosynthetic activity of submerged plants and significantly altering the food chain[2]. Beyond immediate water quality degradation, this issue represents a growing risk to overall ecological balance. Therefore, the treatment of dye-contaminated industrial effluents before discharge is essential to safeguard natural ecosystems[4].

To address this environmental risk, several treatment methods have been explored, such as chemical oxidation, precipitation, membrane filtration, and biological degradation. Nonetheless, many of these approaches are limited by high costs, technical demands, or the generation of hazardous secondary waste[5]. In this context, adsorption stands out as a highly effective option, valued for its ease of operation and excellent performance[6]. Ongoing research increasingly focuses on developing affordable adsorbents to improve the economic feasibility of wastewater treatment. While activated carbons remain the reference material, their high production costs have driven the search for alternative options, including natural clays and zeolites[7]. Zeolites are crystalline aluminosilicates with a three-dimensional porous structure that gives them remarkable ion-exchange and adsorption properties[8]. Although they are traditionally synthesized from high-purity chemical reagents, recent trends favor "green valorization" routes that use silica and alumina-rich materials sourced from natural deposits or industrial waste. This strategy offers a significant opportunity for Côte d'Ivoire, which has abundant underground mineral resources, especially clays and silicate minerals, that provide excellent natural sources of silica and alumina. Recent work has shown that synthesized zeolites perform exceptionally well in removing various pollutants, including anionic and cationic dyes, thanks to their adjustable porosity[9].

This raises a key question: how can the synthesis of zeolitic materials from local natural resources or industrial by-products in Côte d'Ivoire be optimized to yield high-performance, environmentally friendly, cost-effective adsorbents? In response, recent research has concentrated on developing efficient adsorbent substrates for the treatment of wastewater contaminated with persistent organic pollutants, such as industrial dyes. The arm of this study is to assess the effectiveness of a synthetic zeolite as an adsorbent for removing Bezaktiv Orange GO dye from aqueous solutions. More specifically, this work aims to synthesize a zeolite from raw clay, characterize its structural features, and examine its adsorption performance in the removal of Bezaktiv Orange GO dye.

MATERIALS AND METHODS

Raw Material

A kaolin-type clay (Figure 1) was utilized as the primary precursor for zeolite synthesis due to its high silica (SiO_2) and alumina *(*Al_2O_3*)* contents, and natural abundance. The clay sample was collected from M'battra village, located in the Grand Morié sub-prefecture within the Agnéby-Tiassa, region of Côte d'Ivoire (5°56'00" N latitude, 4°13'00" W longitude. The harvested raw sample was sun-dried for 5 days, mechanically ground, and subsequently sieved through a 100 µm mesh to isolate kaolin particles with a size ≤ 100 µm.

Reagents

All reagents employed in this work were of analytical grade and were utilized as received, without additional purification. Sodium hydroxide (99%) was supplied by Expertise Chimique. Hydrochloric acid (37%) and sodium chloride (99%) were purchased from Scharlau, and Bezaktiv Orange GO dye (99%) was acquired from CHT Smart Chemistry (Switzerland). Distilled water was



Fig. 1: Kaolin-type clay

employed for the preparation of all solutions and reagents.

Synthesis of the Zeolite

The preparation of the zeolite from the kaolinic clay was carried out in two main stages: raw clay purification followed by the hydrothermal synthesis process.

Purification of Raw Kaolin

Purification was performed to separate the fine sub-2 µm fraction from the 100 µm sieved kaolin. To accomplish this, a 500 g sample of the clay powder was mixed with 1,000 mL of distilled water (solid/liquid ratio = 1/2). This blend was agitated for 5 min to achieve complete particle dispersion. Gravitational differential sedimentation was then allowed to proceed by leaving the suspension undisturbed for 2 h. During this period, denser mineral contaminants and coarse particles migrated to the bottom, whereas fine aluminosilicate sheets remained stable in the upper phase. The supernatant was carefully recovered by siphoning without disturbing the settled pellet, and then subjected to centrifugation (SIGMA centrifuge, Model 3-16KL) at 2,500 rpm for 15 min. The concentrated, purified kaolin was subsequently dried at 105 °C for a 24 h using a MEMMERT UN 260 drying oven, before being pulverized in an agate mortar to yield a uniform fine powder (Figure 2).

Synthesis of Zeolite from Purified Kaolin

Zeolite synthesis was carried out using a hydrothermal method, beginning with the thermal transformation of kaolin into metakaolin. This step involved calcining the purified clay powder in a muffle furnace at 700 °C for 4 h. Subsequently, 3 g of the resulting metakaolin was combined with 80 mL of a 1 mol/L NaOH aqueous solution. The suspension



Fig. 2. Visual aspect of the purified kaolin powder

was subjected to an aging period of 24 hours at room temperature ((30±2) °C). The aged precursor gel was then transferred to a stainless-steel autoclave and heated in an oven at 105 °C for 9 hours to induce crystallization. The resulting crystalline solid was collected by vacuum filtration, thereby separating it from the alkaline liquid phase. The obtained product was rinsed repeatedly with distilled water until a neutral pH was achieved to eliminate residual sodium hydroxide, and subsequently dried at 105 °C for 24 h. Figure 3 summarizes the different synthesis steps of the zeolitic eco-adsorbent.

Material Characterization

Functional Group Identification

Functional groups present in the purified clay and the synthesized product were characterized by Fourier-transform infrared (FTIR) spectroscopy. Spectra were recorded over a wavenumber range of 500 to 4,000 cm^{-1} with an Agilent Cary 630 FTIR spectrophotometer.

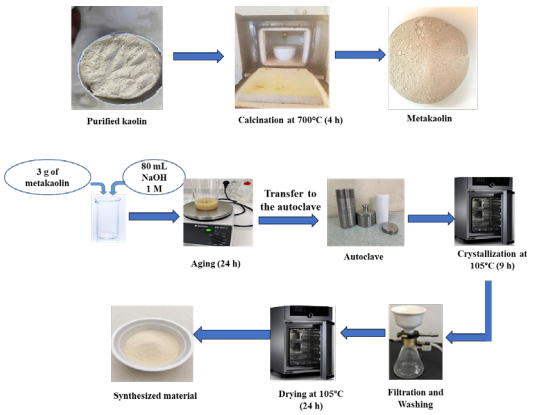


Fig. 3: Synthesis steps of the zeolitic eco-adsorbent

Crystalline Phase Determination

Crystalline phases within the matrices were determined by X-ray diffraction (XRD). Powder diffractograms were collected at a controlled temperature of 25 °C in the 2θ scanning range of 5° to 70°, with a continuous step size of 0.05°, utilizing a Bruker D8 Advance diffractometer.

Determination of the Point of Zero Charge (pH_{PZC})

The pH_{PZC} denotes the pH at which the net surface charge of the zeolite becomes zero. This parameter was determined using the pH drift method [10]. In this procedure, the zeolite was

placed in contact with 50 mL of a 0.1 mol/L NaCl background electrolyte. The initial pH of the solutions was pre-adjusted across a range from 2 to 11 using 1 mol/L HCl and NaOH solutions. Following a 48 h equilibration period under constant stirring, the final pH was recorded. The pH variation ($\Delta pH = pH_f - pH_i$) was plotted against pHi, where the intersection at $\Delta pH = 0$ yielded the experimental pH_{PZC}.

5- Adsorption Experiments

To evaluate the pollutant uptake performance of the synthesized zeolite, adsorption experiments were conducted using Bezaktiv Orange GO as a model industrial dye. Initially, the effect of pH was examined to determine the optimal condition for maximum removal efficiency. To do this, 0.1 g of the prepared adsorbent was contacted with 100 mL of the dye solution under continuous agitation for 60 minutes. The pH of the solution was adjusted from 2 to 10 using 1 mol/L HCl or NaOH. Following separation by filtration, the remaining absorbance was measured at 420 nm with a UV-Vis spectrophotometer (Aqualytic AL800 model). The equilibrium dye concentrations were determined using a linear calibration curve established over a concentration range of 0 to 10 mg/L. The decolorization efficiency R was then calculated using equation 1.

$$R(\%) = \left(\frac{C_0 - C_r}{C_0} \right) \times 100 \quad ...(1)$$

Where C_0 (mg/L) and C_r (mg/L) represent the initial and residual dye concentrations, respectively.

Kinetic experiments were performed by introducing 0.5 g of the synthesized material into 500 mL of the dye solution pre-adjusted to pH = 2. Aliquots were sampled at regular time intervals, and each collected sample was filtered. The absorbance of the filtrate was measured using a UV-Vis spectrophotometer at 420 nm to determine the residual dye concentrations as described previously. The adsorption capacity of the material was calculated using Equation 2.

$$q_t = \left(\frac{C_0 - C_r}{m} \right) \times V \quad ...(2)$$

Where C_0 (mg/L) is the initial concentration of the target solution, C_t (mg/L) represents the concentration at time t, m (g) denotes the mass of the adsorbent, and V (L) is the volume of the solution undergoing treatment.

The effect of the initial dye concentration was evaluated under identical experimental conditions. For the adsorption isotherm study, batch experiments were conducted at room temperature ((30 ±2) °C) by contacting 0.1 g of the synthesized material with 100 mL of dye solutions at various concentrations ranging from 25 to 1000 mg/L. The solutions were maintained at pH = 2 and continuously agitated using an Innova shaker for 24 h to ensure that equilibrium was reached.

RESULTS AND DISCUSSION

Properties of the Synthesized Material

Surface Functional Groups

Figure 4 illustrates the FTIR spectra corresponding to the purified kaolin and synthesized material.

The observed differences confirm the structural transformation of the kaolin raw material. The detected bands were assigned based on literature data. The band at 413 cm^{-1} recorded in the spectrum of the synthesized material corresponds to the silicate tetrahedron, indicating the presence of an O–Si–O bending vibration [11]. The appearance of the peaks at 434 cm^{-1} and 549 cm^{-1} provides clear evidence of both symmetric and asymmetric T–O–T (T = Si or Al) stretching modes. These modes involve the internal (SiO_4 et AlO_4) tetrahedral units and are specifically associated with the ring structures of the zeolite framework [12–15].

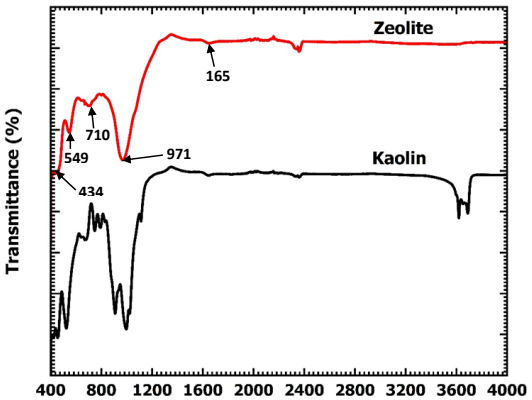


Fig. 4: FTIR spectra of the purified kaolin and the synthesized material

The peak recorded at 710 cm^{-1} is attributed to the skeletal stretching modes of the aluminosilicate framework. This spectral feature underscores a significant structural rearrangement, signifying the transition of aluminum from an octahedral environment in raw kaolinite to the tetrahedral coordination typical of metakaolin[13]. This signal further verifies the silico-aluminous nature of the prepared matrix. Additionally, the absorption band within the 900–1,000 cm^{-1} region becomes distinctly more pronounced and exhibits a slight redshift toward lower frequencies. Such a spectral evolution indicates a clear rearrangement of the aluminosilicate lattice. Thus, the prominent peak centered at 971 cm^{-1} is unambiguously attributed to the fundamental stretching vibrations of the zeolitic framework[16]. This band is attributed to the Si–O and Al–O bending vibrations. Furthermore, the absorption band observed around 1,600 cm^{-1} can be assigned to the hydroxyl groups (–OH, Si–OH, or Al–OH) located on the zeolite surface[13,17].

X-ray Diffraction (XRD) Analysis

The X-ray diffractograms of the purified kaolin and the synthesized material are shown in Figure 5.

The structural analysis assessed by XRD reveals the total disappearance of the baseline kaolinite reflection at 2θ = 12.3°. This structural change confirms the effectiveness of the thermal activation, indicating full dehydroxylation of the kaolinite lattice into a highly disordered, reactive metakaolin phase [18]. Conversely, a prominent and narrow diffraction peak is observed at 2θ = 26.6°, along with a secondary reflection of lower intensity at 2θ = 20.8°, both identifying the crystalline presence of quartz impurity. The preservation of these reflections implies that the raw material possessed a substantial amount of crystalline silica, which behaved as a chemically inert component that resisted both calcination and hydrothermal aging. Concurrently, the growth of new well-defined and intense reflections at 2θ = 17.8°, 35.8° et 45.1° demonstrates successful nucleation and crystallization kinetics[19]**.** These peaks mark the transition from an initially amorphous aluminosilicate gel to a highly ordered three-dimensional solid phase. The extracted 2Δpositions perfectly match the standard diffraction fingerprint of a P-type zeolite (GIS symmetry) or sodalite [11,12].

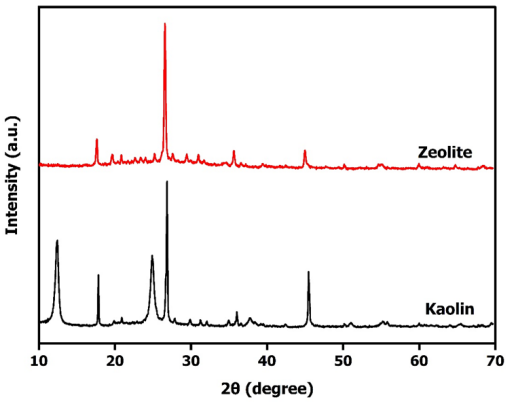


Fig. 5: **X-ray diffraction patterns of the purified kaolin and the synthesized material**

Determination of pH_{PZC}

The evaluation of the pH_{PZC} provides critical insights into the acidic or basic nature of the adsorbent's surface sites. The obtained data profile is plotted in Figure 6.

As illustrated by the data plot, the experimental pH_{PZC} of the prepared zeolite was determined to be 6.08. This value is comparable to those reported in the literature for zeolites, which generally range between 5 and 7 depending on their chemical compositions and synthesis conditions [20,21]. Consequently, at a solution pH above 6.08, the material surface exhibits a net negative charge. Conversely, at a pH below 6.08, the surface becomes positively charged. Finally, a neutral surface condition is maintained precisely at pH = 6.08.

Effect of pH on Bezaktiv Orange GO Adsorption

As illustrated in Figure 7, the removal

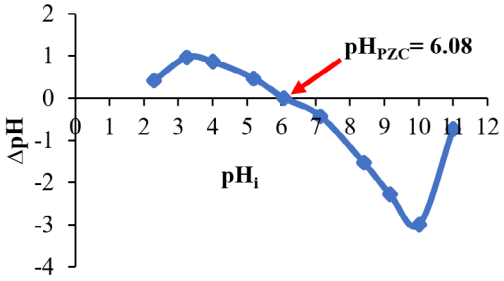


Fig. 6. Plot of pH variation versus initial pH

efficiency of Bezaktiv Orange GO dye by the synthesized zeolite highly depends on the solution pH.

An increase in solution pH leads to a sharp decline in dye retention, which reaches minimal levels under neutral and alkaline conditions. This behavior directly correlates with the zeolite's point of zero charge (pH_{PZC} = 6.08). In highly acidic media (pH < pH_{PZC}), protonation of the surface functional groups imparts a net positive charge to the zeolitic material. This state promotes strong attractive electrostatic interactions with the anionic species of the dye. Conversely, under regimes where the pH exceeds 6.08, surface deprotonation induces a negative surface charge, triggering electrostatic repulsion and a consequent drop in adsorption capacity. The peak removal efficiency of 84.3% is achieved at pH = 2. These findings confirm that the uptake of Bezaktiv Orange GO by the synthesized zeolite is highly favored in acidic environments and primarily dictated by electrostatic forces. Comparable trends have been documented in several investigations involving the adsorption of anionic dyes onto zeolitic materials [22]

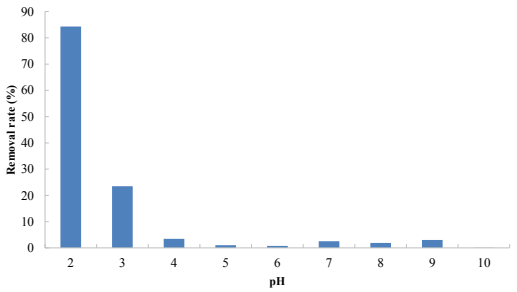


Fig. 7: Influence of solution pH on the removal percentage of the dye

specific concentration was selected for subsequent experimental steps.

Kinetic Study of Bezaktiv Orange GO Dye Adsorption onto the Zeolite

To evaluate the adsorption kinetics, a 25 mg/L Bezaktiv Orange GO dye solution was employed. The profile illustrating the amount of retained dye versus the adsorption time is presented in Figure 9.

Dye adsorption occurs rapidly during the first 30 minutes of contact, followed by a slower progression until a stable plateau is reached at

Effect of Initial Dye Loading on the Adsorption Process

Figure 8 shows the adsorption kinetics of Bezaktiv Orange GO on the synthesized zeolite for different initial concentrations (ranging from 25 to 500 mg/L).

Elevating the initial dye loading results in a corresponding decline in the overall removal efficiency. At lower concentrations, the ratio of target dye molecules to vacant surface sites remains low, which facilitates comprehensive adsorption. Conversely, under high-concentration regimes, the active binding sites of the zeolite undergo progressive saturation, thereby restricting further pollutant sequestration. This trend is commonly documented during dye immobilization on zeolitic substrates and stems from intensified competitive interactions among dye ions for the remaining available sites [23,24]. Optimal performance was recorded at a dye concentration of 25 mg/L, yielding

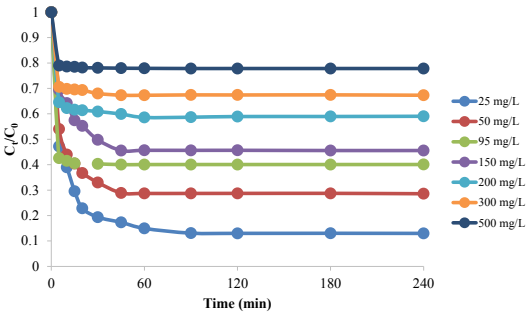


Fig. 8: Variation of dye concentration as a function of contact time

90 minutes. This rapid initial phase is due to the abundance of vacant active sites on the adsorbent surface, which facilitates the rapid immobilization of the dye molecules. Comparable kinetic behavior was reported by Salah Elbanna *et al.* [25]a naturally occurring zeolite with unique adsorption properties, is investigated in its nanoscale form as a sustainable adsorbent for effectively removing contaminant dyes, rhodamine B (RhB during their study on the adsorption of dyes onto natural and synthetic zeolites. The subsequent slowing-down phase generally results from the progressive saturation of these active sites, as well as from limitations related to intraparticle diffusion. The latter phenomena

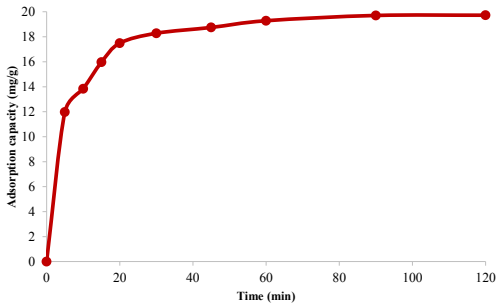


Fig. 9: Change in the amount of dye adsorbed over time

become predominant as the dye molecules migrate towards the zeolite's internal porous network [23,24].

To elucidate the underlying pathways governing the adsorption process, both pseudo-first-order and pseudo-second-order kinetic models were fitted to the gathered experimental data. Equilibrium is reached after 90 minutes with an equilibrium adsorption capacity ($q_{e,exp}$) of 19.707 mg/g. All the kinetic constants and parameters calculated from these models are summarized in Table 1.

The experimental data are more accurately matched by the pseudo-second-order kinetic framework, as evidenced by the higher R2 value. To ensure a robust validation, a comparative statistical evaluation was performed between the two models. thus, the chi-squared (χ^2), non-linear test, defined by equation 3, was employed to quantify the goodness-of-fit of the kinetic profiles[26].

$$\chi^2 = \frac{(q_{e,\exp} - q_{e,cal})^2}{q_{e,cal}} \quad ...(3)$$

Where $q_{e,cal}$, is the theoretical equilibrium adsorption capacity calculated from the kinetic model.

A significant divergence is observed between the experimental adsorption capacity ($q_{e,exp}$ = 19.707 mg/g) and the calculated theoretical value derived from the pseudo-first-order simulation ($q_{e,cal}$ = 10.780 mg.g^{-1}). In contrast, the pseudo-second-order approach yields a calculated value ($q_{e,cal}$ = 20.242 mg.g^{-1}) in excellent agreement with experimental measurements. This observation is reinforced by the noticeably smaller Δ error index registered for the pseudo-second-order framework compared to the pseudo-first-order one. This good fit, corroborated by a coefficient of determination close to 1 (R^2 = 0.998), validates the applicability of the pseudo-second-order model for describing the adsorption kinetics of the Bezaktiv Orange GO dye. Therefore, these findings confirm that the adsorption is governed by chemisorption [27]only the chemical product has an influence on the adsorption capacity of the activated carbons. Two activated carbons (bpAC and ACB.

Adsorption Isotherm Study

Figure 10 illustrates the plot of equilibrium adsorption capacity as a function of equilibrium concentration.

Based on IUPAC classification, the data plot fits a Type III isotherm configuration, which is characterized by a low initial affinity at lower concentrations (C_e < 100 mg/L), followed by a continuous increase in the adsorption capacity. The experimental equilibrium data were simulated using the Langmuir and Freundlich equations to decipher the adsorption mechanism of Bezaktiv Orange GO dye onto the zeolite. Determination coefficients and computed models' parameters are compiled in Table 2.

Although the Langmuir model exhibits the highest coefficient of determination (R^2 = 0.997), it generates physically anomalous values

Table 1: Kinetic parameters and determination coefficients derived from the pseudo-first and pseudo-second-order models

Pseudo-first-order kinetic model				Pseudo-second-order kinetic model			
R^2	K_1 (min^{-1})	qe,cal (mg/g)	χ^2	R^2	K_2 (g/mg.min)	qe,cal (mg/g)	χ^2
0.929	0.0056	10.780	7.392	0.998	0.0163	20.242	0.014

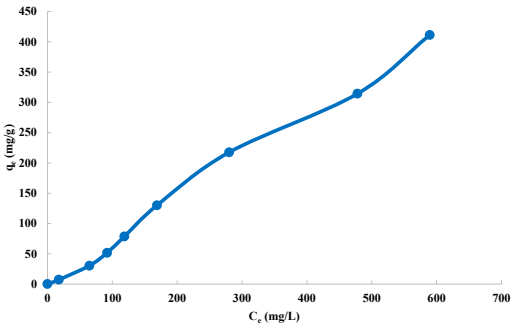


Fig. 10: **Profile of equilibrium Bezaktiv Orange GO dye adsorption versus equilibrium solution concentration**

characterized by negative maximum adsorption capacity and affinity constant parameters. This phenomenon, frequently encountered during the linear fitting of highly heterogeneous systems, invalidates the assumption of ideal monolayer coverage on energetically equivalent sites. These theoretical findings perfectly corroborate the geometric profile of figure 10. The upward concavity of the curve at lower concentrations explains the mathematical failure of the Langmuir model under linear regression. Conversely, this geometry

Table 2: Langmuir and Freundlich adsorption isotherm constants for Bezaktiv Orange GO dye

Models	Constants	Values
Langmuir	R^2	0.997
	qm (mg/g)	-192.307
	K_L (L/mg)	-0.002
Freundlich	R^2	0.990
	K_F (mg/(g. ($L^{1/n}$. $mg^{-1/n}$))	0.268
	1/n	1.166

validates the applicability of the Freundlich model, where the heterogeneity parameter 1/n (1.166) exceeds unity. Such a configuration serves as the signature of a cooperative adsorption mechanism, corresponding to a Type III isotherm according to the IUPAC classification [28]**.** This behavior indicates that the immobilization of the initial dye molecules alters the zeolite's surface environment, generating new, more active sites that facilitate subsequent solute binding through intermolecular Van der Waals forces or $\pi-\pi$ interactions[29].

CONCLUSION

In summary, a high-performance zeolitic eco-adsorbent was successfully engineered through the hydrothermal conversion of local kaolin clay and applied as an efficient substrate to remove Bezaktiv Orange GO dye from aqueous solution. FTIR and XRD structural analysis confirmed the successful formation of a crystalline, porous zeolitic material featuring a well-developed network of channels and cavities highly conducive to adsorption phenomena. The pH_{PZC} determined was 6.08. Batch adsorption assays revealed that the removal efficiency is dependent on the medium's pH, achieving a peak removal yield of 84.3% at pH = 2. Kinetic investigations indicated that equilibrium was established within 90 minutes, with adsorption capacity of 19.707 mg/g. Furthermore, the adsorption process obeyed the pseudo-second-order kinetic model (R^2 = 0.998), underscoring that the process is predominantly mediated by chemical interactions. Isotherm adsorption modeling showed that the Freundlich equation provided the best mathematical fit, reflecting a multilayer adsorption mechanism across a structurally heterogeneous surface. The kaolin-derived zeolite exhibits promising potential as a cost-effective and efficient substrate for the remediation of organic pollutants in wastewater, particularly for the treatment of dye-bearing textile effluents.

ACKNOWLEDGEMENTS

The authors are thankful to Nangui ABROGOUA University and its Central Laboratory for their essential technical backing and for making available the facilities used in this investigation.

Conflict of Interest

No competing financial interests or personal relationships exist among the authors that could influence or bias the findings reported in this study.

Funding Source

This investigation was entirely self-supported by the authors, and no external financial assistance or grants were provided by third-party organizations.

Data Availability Statement

The data that support the findings of this research are available from the authors upon request.

Ethical Approval Statement

All authors provide their full and unconditional consent for the publication of this research work in the journal.

Informed Consent Statement

Every listed author has read, approved, and authorized the submission of the current manuscript to this journal

Authors' Contributions

Affoué Tindo Sylvie KONAN

Original draft preparation, Writing, Data curation, Software, Visualization

N'Goran Sévérin EROI

Formal analysis, Writing, Software

Ignace Christian M'Bra

Review and editing, Formal analysis, Visualization

Aboubakar Siddik COULIBALY: Investigation

Koffi Siméon KOUADIO: Investigation

Sirata Ibrahima Francis SORO: Investigation, Visualization

Lynda EKOU: Conceptualization, Methodology

Tchirioua EKOU: Supervision, Validation

REFERENCES

1. Tkaczyk, A.; Mitrowska, K.; Posyniak, A. A Review. *Science of The Total Environment* **2020**, *717*, 137222. https://doi.org/10.1016/j.scitotenv.2020.137222.
2. Islam, Md. M.; Aidid, A. R.; Mohshin, J. N.; Mondal, H.; Ganguli, S.; Chakraborty, A. K. *Cleaner Chemical Engineering* **2025**, *11*, 100165. https://doi.org/10.1016/j.clce.2025.100165.
3. Al-Tohamy, R.; Ali, S. S.; Li, F.; Okasha, K. M.; Mahmoud, Y. A.-G.; Elsamahy, T.; Jiao, H.; Fu, Y.; Sun, J. *Ecotoxicology and Environmental Safety* **2022**, *231*, 113160. https://doi.org/10.1016/j.ecoenv.2021.113160.
4. Zemouri, K.; Zougagh, D.; Bouariche, Z.; Belaid, T. Thesis, université Abderrahmane Mira- Bejaia, 2019. http://univ-bejaia.dz/xmlui/handle/123456789/15128.
5. Gavrila□, S.; Ger□cs, T.; Chereji, B.-D.; Munteanu, F.-D. *Water* **2026**, *18* (3), 350. https://doi.org/10.3390/w18030350.
6. Dutta, S.; Gupta, B.; Srivastava, S. K.; Gupta, A. K. A Critical Review. *Mater. Adv.* **2021**, *2* (14), 4497–4531. https://doi.org/10.1039/d1ma00354b.
7. de Magalhães, L. F.; da Silva, G. R.; Peres, A. E. C. *Adsorption Science & Technology* **2022**, *2022*, 4544104. https://doi.org/10.1155/2022/4544104.
8. Kordala, N.; Wyszkowski, M. *Molecules* **2024**, *29* (5), 1069. https://doi.org/10.3390/molecules29051069.
9. Abas, K. M.; Fathy, N. A. *Int. J. Environ. Sci. Technol.* **2024**, *21* (5), 5165–5184. https://doi.org/10.1007/s13762-023-05347-0.
10. Soro, S. I. F.; Konan, A. T. S.; M'bra, I. C.; Kouadio, K. S.; Aketchi, T. L.; Djè, D. Y.; Ekou, L.; Ekou, T. *Orient J Chem 2026* **2026**, *42* (2), 626–638. https://doi.org/10.13005/ojc/420223.
11. Ndlovu, N. Z. N.; Ameh, A. E.; Petrik, L. F.; Ojumu, T. V. *Materials Today Communications* **2023**, *34*, 105436. https://doi.org/10.1016/j.mtcomm.2023.105436.
12. Abdul, H.; Yusuf, W.; Misbakhul, F.; Tri, E. P.; Tri, W.; Dayi Febriana. *RSC Advances* **2025**, *15* (54), 46613–46626. https://doi.org/10.1039/d5ra05960g.
13. Adamou, I. A.; Ibrah, L. A.; Amadou Kiari, M. N.; Manzola, A. S.; Yao, K. B.; Soro, Y. *Int. J. Adv. Res.* **2026**, *14* (05), 1368–1391. https://doi.org/10.21474/IJAR01/23541.
14. Bouna, L.; Ait El Fakir, A.; Benlhachemi, A.; Draoui, K.; Ezahri, M.; Bakiz, B.; Villain, S.; Guinneton, F.; Elalem, N. *Applied Clay Science* **2020**, *196*, 105764. https://doi.

org/10.1016/j.clay.2020.105764.
15. Novembre, D.; Gimeno, D.; Del Vecchio, A. *Sci Rep* **2021**, *11* (1), 4872. https://doi.org/10.1038/s41598-021-84383-7.
16. Rahman, A.; Budi, S.; Kusumaningrum, N.; Prasetyanto, E. A.; Usman, A. *EPJ Web Conf.* **2026**, *377*, 01006. https://doi.org/10.1051/epjconf/202637701006.
17. Asghari, A.; Khorrami, M. K.; Kazemi, S. H. *Sci Rep* **2019**, *9* (1), 17526. https://doi.org/10.1038/s41598-019-54089-y.
18. Kouadio, K. S.; Tchirioua, E.; Dhainaut, J. *Catalysts* **2025**, *15* (2), 188. https://doi.org/10.3390/catal15020188.
19. Liu, Y.; Zhang, B.; Fahimizadeh, M.; Yu, T.; Ou, Z.; Peng, Z.; Yuan, P. *Applied Clay Science* **2025**, *271*, 107796. https://doi.org/10.1016/j.clay.2025.107796.
20. Lastimado, A. E.; Pahunang, R. R.; Rabongue, A.; Buonerba, A. *Journal of Water Process Engineering* **2025**, *79*, 109065. https://doi.org/10.1016/j.jwpe.2025.109065.
21. KragoviΔ M.; StojmenoviΔ M.; PetroviΔ J.; Loredo, J.; PašaliΔ S.; NedeljkoviΔ A.; RistoviΔ I. *Procedia Manufacturing* **2019**, *32*, 286–293. https://doi.org/10.1016/j.promfg.2019.02.216.
22. Salzano de Luna, M.; Greco, F.; Pastore, R.; Mensitieri, G.; Filippone, G.; Aprea, P.; Mallamace, D.; Mallamace, F.; Chen, S.-H. *International Journal of Molecular Sciences* **2021**, *22* (11), 5535. https://doi.org/10.3390/ijms22115535.
23. Dehmani, Y.; Mohammed, B.; Oukhrib, R.; Dehbi, A.; Lamhasni, T.; Brahmi, Y.; El-Kordy, A.; Franco, D.; Georgin, J.; Lima, E.; Alrashdi, A.; Tijani, N.; Abouarnadasse, S. A Critical Review. *Arabian Journal of Chemistry* **2023**, *17*, 105474. https://doi.org/10.1016/j.arabjc.2023.105474.
24. Imessaoudene, A.; Cheikh, S.; Hadadi, A.; Hamri, N.; Bollinger, J.-C.; Amrane, A.; Tahraoui, H.; Manseri, A.; Mouni, L. *Separations* **2023**, *10* (1), 57. https://doi.org/10.3390/separations10010057.
25. Salah Elbanna, E.; Farghali, A. A.; Khedr, M. H.; Taha, M. *Journal of Molecular Liquids* **2024**, *409*, 125538. https://doi.org/10.1016/j.molliq.2024.125538.
26. Nayak, A. K.; Pal, A. *Journal of Molecular Liquids* **2019**, *276*, 67–77. https://doi.org/10.1016/j.molliq.2018.11.089.
27. Konan, A. T. S.; Richard, R.; Andriantsiferana, C.; Yao, K. B.; Manero, M.-H. *Journal of Materials and Environmental Science* **2020**, *11* (10), 1584–1598.
28. Shimizu, S.; Matubayasi, N. *Langmuir* **2023**, *39* (39), 13820–13829. https://doi.org/10.1021/acs.langmuir.3c01243.
29. de Santana, J. E.; dos Santos Neto, A. E.; de Andrade, F. G. S.; Ferreira, A. F.; Ghislandi, M. G.; da Motta Sobrinho, M. A. *Environ Sci Pollut Res* **2026**, *33* (7), 2852–2885. https://doi.org/10.1007/s11356-026-37455-y.